Supporting Information

TiO_2 protection layer and well-matched interfaces enhance stability of $Cu_2ZnSnS_4/CdS/TiO_2$ for visible water splitting

Xuqiang Zhang[a,b], Gongxuan Lu[b*], Yuqi Wu[b], Jiali Dong[a], Chenwei Wang[a*]

[a]State Key Laboratory for Oxo Synthesis and Selective Oxidation, Lanzhou Institute of Chemical Physics, Chinese Academy of Sciences, Lanzhou, 730000, China

[b]Key Laboratory of Atomic and Molecular Physics & Functional Materials of Gansu Province, College of Physics & Electronic Engineering, Northwest Normal University, Lanzhou 730070, China

* Corresponding author.
E-mail address: gxlu@lzb.ac.cn (G. Lu), cwwang@nwnu.edu.cn (C. Wang).

Photocatalytic hydrogen evolution activity test: In the typical PHE reaction of CZTS/CdS/TiO_2/Pt, the sealed pyrex flask contained 70 mg photocatalyst, which were dispersed into 100 mL de-ionized H_2O using ultrasound treatment for 10 min. Then the reaction system was degassed by bubbling Ar gas for 30 min. In order to get the detailed hydrogen production performance of the catalyst, the produced gas composition were detected every 30 min under visible light irradiation.

Stability test: The cyclic stability of PHE over the catalyst was performed under the same reaction vessel and light conditions. After going through a complete photocatalytic reaction, the photocatalytic reaction system was degassed again using Ar gas. Then the photocatalytic system was irradiated again.

H_2 and O_2 back reaction test: The back experiments of H_2 and O_2 over the CZTS/CdS/TiO_2/Pt catalyst was carried out in the same container, which contained 70 mg CZTS/CdS/TiO_2/Pt and 100 mL of de-ionized H_2O. Subsequently, the suspension was treated with ultrasound for 30 min and degassed using Ar gas to exclude the air inside. To prove that the reverse recombination reaction of H_2 and O_2 is ubiquitous, 1 mL O_2 and 1 mL H_2 were injected into sealed Pyrex flask. The back reaction was carried out under dark condition and the corresponding recombination rate was tested by measuring of decreased amount of hydrogen and oxygen.

AQEs test: AQEs of photocatalysts was measured under a series of visible wavelengths with specific wavelengths, 430, 460, 490, 520, and 550 nm, by a set of bandpass filters. The reaction conditions are the same as the photocatalytic hydrogen production illumination for 2 h with bandpass filters. The AQEs of photocatalysts were calculated based on the following equation (1):

$$\text{AQEs } [\%]=(2N_{H2}/N_p)\times 100\% \quad (1)$$

where $2N_{H2}$ was the number of electrons participating in the reaction; and N_p is the total number of incident photons that was determined using a ray virtual radiation actinometer (FU 100).

Isotopes tracer experiments*:* The isotopes tracer experiments of CZTS/CdS/TiO_2/Pt photocatalyst were carried out in a downsized reactor to confirm the overall water splitting and form simultaneously H_2 and O_2. In this part, the de-ionized H_2O was replaced by high purity D_2O and $H_2{}^{18}O$. Due to the proportional reduction of the reaction system, the light irradiation time of isotopes tracer experiments was extended to 4 h, and the gas composition was analyzed using a high sensitivity Gas Chromatography-Mass Spectrometer (TILON-LC-D200 M).

Photoelectrochemical measurements*:* All the electrochemical measurements were measured on an electrochemical analyzer (CHI660A) in a standard three-electrode cell, consisting of an organic glass enclosure with a quartz window and a 1.2 cm diameter opening opposite the window to the work electrode clamped. The working electrodes were prepared by drop-coating Nafion-impregnated sample suspensions directly onto the precleaned ITO glass surface. 10 mg of material were ultrasonically dispersed into 2.0 mL of 2-propanol solution containing Nafion (5 wt%, DuPont) for 30 min to form a homogenous ink; 10 mL of the ink were coated on the ITO and dried at 50 °C for 30 min. The area of the working electrode exposed to the electrolyte was about 1 cm^2. A saturated calomel electrode (SCE) was used as the reference electrode and a Pt foil as the

counter electrode, respectively. All electrochemical measurements, including Mott-Schottky plots, transient photocurrent-time profile, electrochemical impedance spectroscopy (EIS), polarization curves and chronopotentiogram profile of samples were performed at room temperature in 0.5 M Na_2SO_4 aqueous. A 300-W Xe lamp equipped with an optical cutoff filter of 420 nm was used for the light source.

***Morphology and structural characterizations**:* A transmission electron microscope (TEM, ecnai-G2-F30), high angle annular dark field scanning transmission electron microscopy (HAADF-STEM) and elemental mapping images were used to study the structure and elements distribution. The crystallinity of the specimens was analyzed by x-ray diffraction (XRD) using a Rigaku B/Max-RB diffractometer with a nickel filtrated Cu Kα radiation. Micro-Raman measurements were conducted using a Horiba HR800 Raman system at room temperature, and the 632.8 nm line from a He-Ne laser was used as the excitation laser. The chemical composition of the samples was characterized by x-ray photoelectron spectroscopy (XPS, PHI-5702) using Al Kα monochromatic radiation. The specific surface areas of the catalysts were determined by N_2 adsorption-desorption measurements by employing the Brunauer-Emmet-Teller (BET) method (Micromeritics apparatus ASAP 2020M) at 77 K. Thermal gravimetric (TG) analysis was performed on a NETZSCH STA 449F3 thermogravimetric/differential thermal analyzer by heating the samples at 10 °C/min to 600 °C in the nitrogen condition. Ultraviolet-visible (UV-vis) diffuse reflectance spectra (DRS) were obtained with a Hewlett-Packard 8453 spectrophotometer in which $BaSO_4$ powder was used as the internal standard to obtain the optical properties of the samples. The electron transport properties of the samples were measured by the two-probe method on a Keithley 4200 semiconductor characterization system. Carrier concentration, mobility and resistivity were evaluated by Hall effect measurements at room temperature in a Van der Pauw four-point probe configuration with a magnetic induction of 0.55 T (Quantum Technology Corp., Blaine WA, USA). The inductively coupled plasma-optical emission spectrometer (ICP-OES) was performing on Agilent 725-ES unit. Fluorescence lifetime measurements were performed on a Horiba Jobin Yvon Data Station HUB operating in time-correlated single photon counting mode (TCSPC) with a time resolution of 200 ps. Nano LED diode emitting pulses at 464 nm with 1 MHz repetition rate were used as an excitation source. Isotope tracer experiments have been performed in a sealed Pyrex reactor by measuring D_2 using a gas chromatography mass spectrometer (GC-MS, MAT 271).

Table S1. The textural properties of the CZTS, CZTS/CdS and CZTS/CdS/TiO_2 catalysts obtained from BET method.

Samples	S_{BET} (cm^2/g)	Pore volume (cm^3/g)	Average pore size (nm)
CZTS	23.84	0.03	5.4
CZTS/CdS	10.33	0.05	15.8
CZTS/CdS/TiO_2	8.13	0.04	15.5

Table S2. The bond length between atoms (L), interface surface area (S), superlattice binding energy (E_{BE}), and adhesion energy (E_{AE}) in the constructed six structures: CZTS(001), CdS(111), TiO_2(001), CZTS(001)-CdS(111), CdS(111)-TiO_2(001) and CZTS(001)-TiO_2(001) superlattices.

Samples	CZTS(001)	CdS(111)	TiO_2(001)	CZTS(001)/ CdS(111)	CdS(111)/ TiO_2(001)	CZTS(001)/ TiO_2(001)
L (Å)	L_{Cu-S}=2.288 L_{Zn-S}=2.362	L_{Cd-S}=2.525	L_{Ti-O}=1.971	L_{Cu-S}=2.421 L_{Zn-S}=2.542 L_{Cd-S}=2.616	L_{Cd-S}=2.685 L_{Ti-O}=1.983 L_{Cd-O}=2.170	L_{Cu-S}=2.532 L_{Zn-S}=2.417 L_{Ti-O}=2.332 L_{Ti-S}=2.651
S ($Å^2$)	--	--	--	33.99	33.99	21.16
E_{BE} (eV)	-61.35	-22.32	-30.89	-117.70	-85.61	-100.39
E_{AE} ($eVÅ^{-2}$)	--	--	--	-1.001	-0.953	-0.385

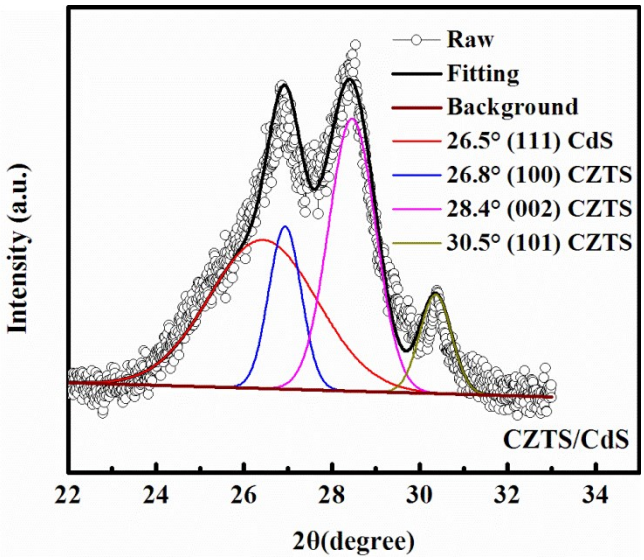

Fig. S1 A multiple Lorentzian peak fitting reflection of CdS and CZTS at 2θ from 22.0° to 33.0° in the CZTS/CdS photocatalyst.

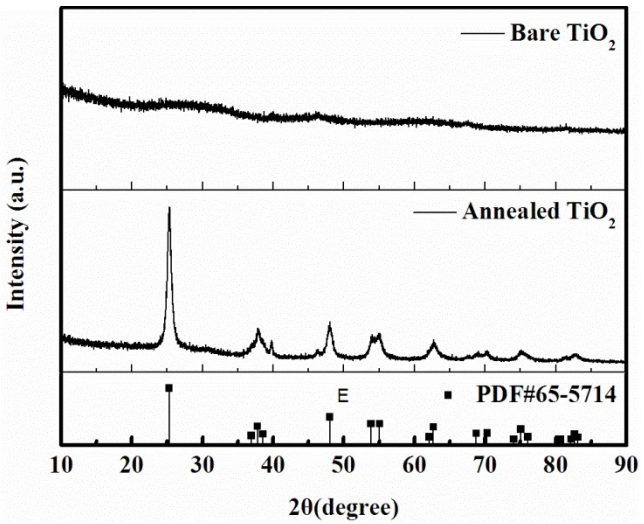

Fig. S2 XRD pattern of bare TiO_2 and annealed TiO_2. It can be clearly found that the bare TiO_2 is amorphous using hydrolysis of titanium tetraisopropanoiate.

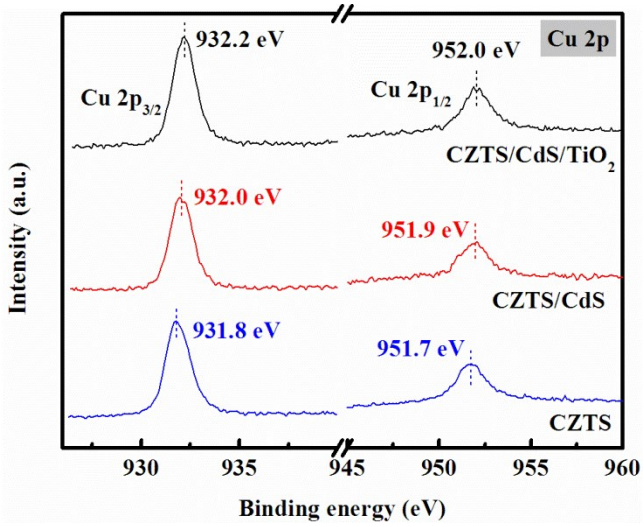

Fig. S3 High-resolution Cu 2p XPS spectra of the CZTS, CZTS/CdS and CZTS/CdS/TiO_2 photocatalysts.

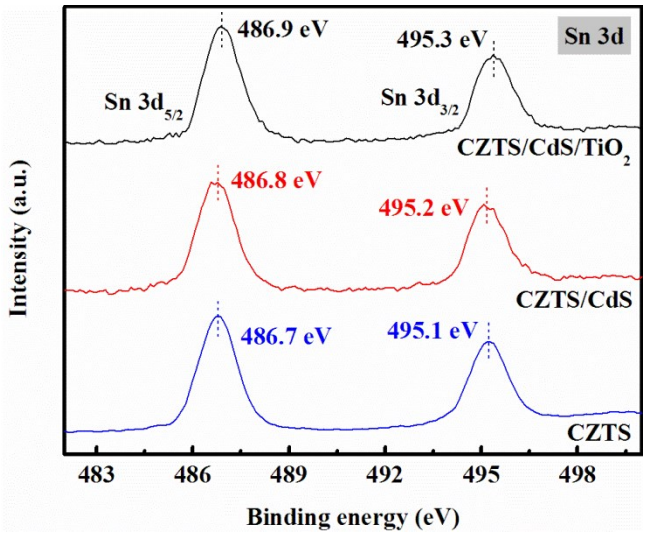

Fig. S4 High-resolution Sn 3d XPS spectra of the CZTS, CZTS/CdS and CZTS/CdS/TiO_2 photocatalysts.

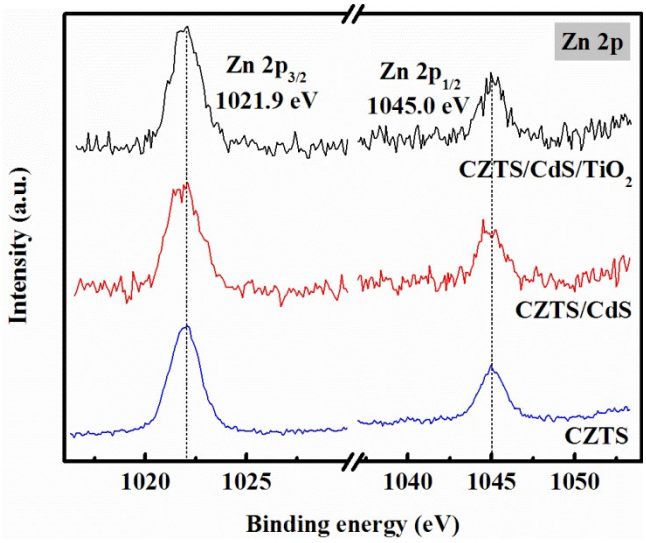

Fig. S5 High-resolution Zn 2p XPS spectra of the CZTS, CZTS/CdS and CZTS/CdS/TiO_2 photocatalysts.

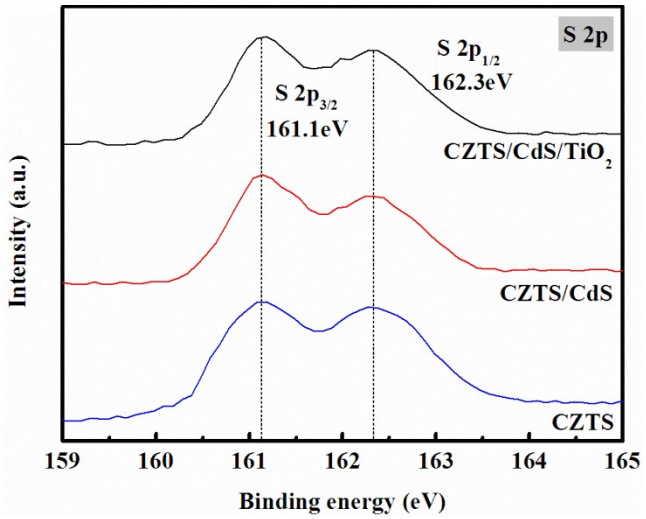

Fig. S6 High-resolution S 2p XPS spectra of the CZTS, CZTS/CdS and CZTS/CdS/TiO_2 photocatalysts.

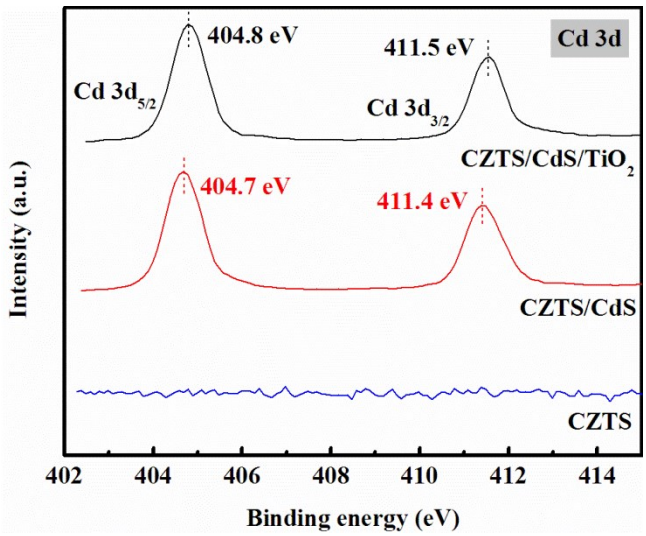

Fig. S7 High-resolution Cd 3d XPS spectra of the CZTS, CZTS/CdS and CZTS/CdS/TiO_2 photocatalysts.

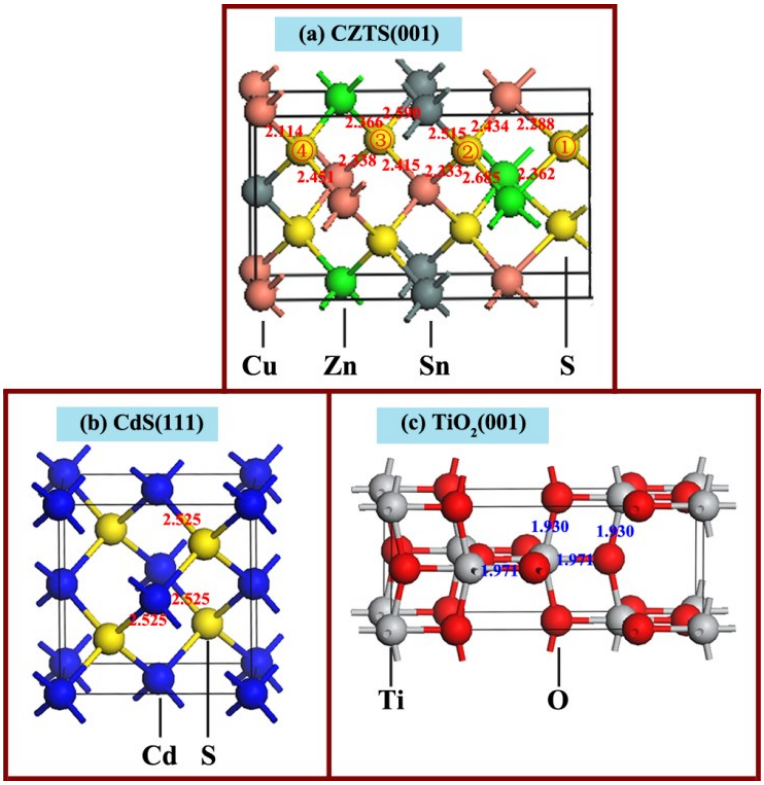

Fig. S8 Superlattices (a) wurtzite-CZTS(001), (b) cubic-CdS(111) and (c) anatase-TiO_2(001).

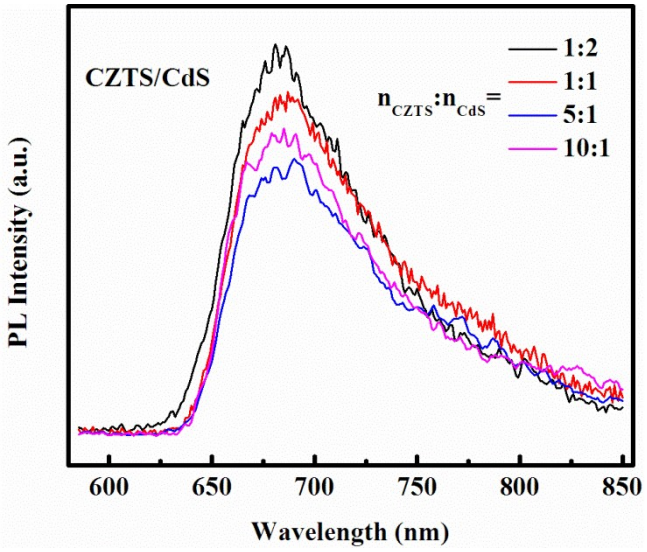

Fig. S9 PL spectra of different molar ratio of CZTS and CdS in the CZTS/CdS catalyst.

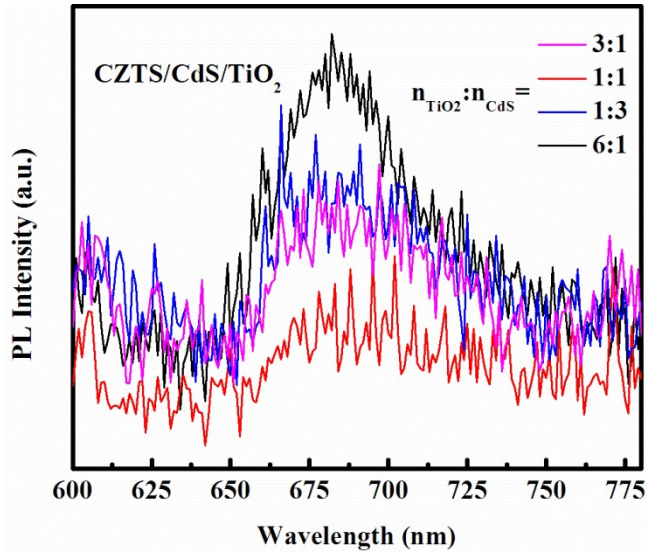

Fig. S10 PL spectra of different molar ratio of CdS and TiO_2 in the CZTS/CdS/TiO_2 catalyst..

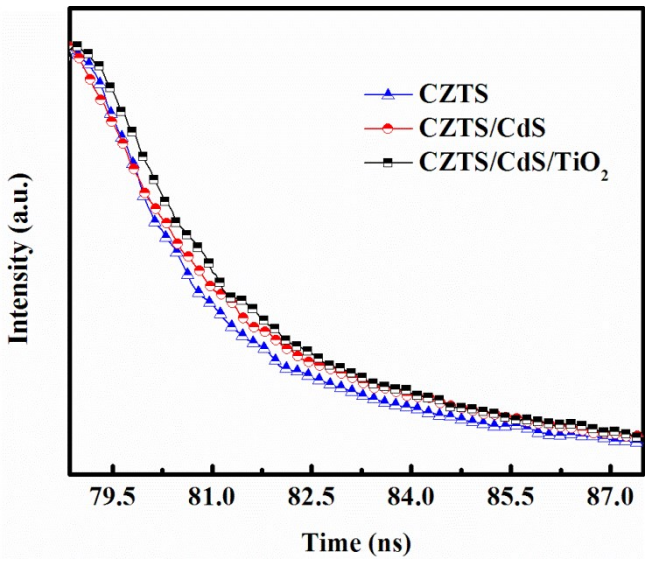

Fig. S11 Time-resolved PL decay curves of the CZTS, CZTS/CdS and CZTS/CdS/TiO_2 catalysts.

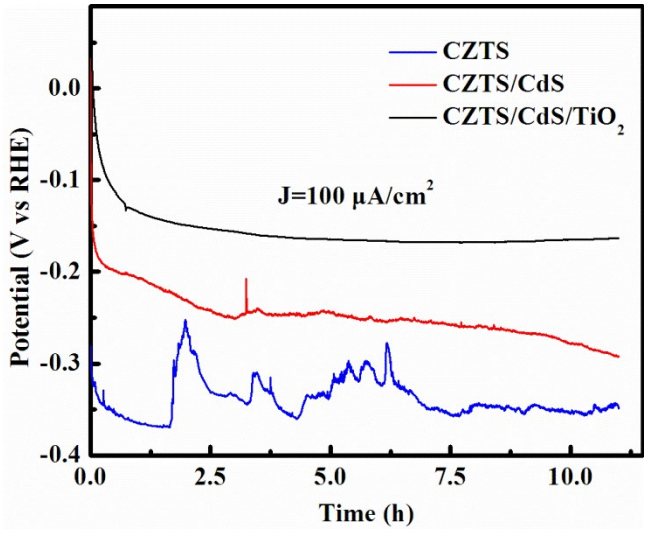

Fig. S12 Chronopotentiogram profile of the as-prepared CZTS, CZTS/CdS and CZTS/CdS/TiO_2 films on ITO glass in 0.5 M Na_2SO_4 aqueous under a constant impressed current density of 100 μA cm^{-2}.

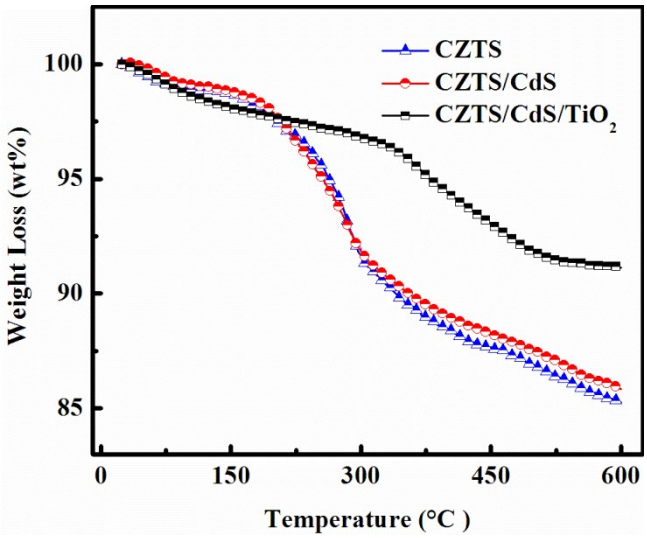

Fig. S13 Thermogravimetric analysis of the synthesized CZTS, CZTS/CdS and CZTS/CdS/TiO_2 catalysts.

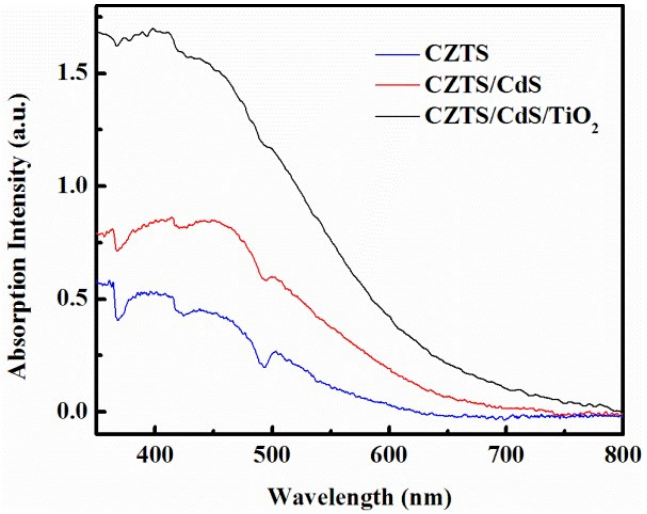

Fig. S14 UV-vis absorption spectra of the CZTS, CZTS/CdS and CZTS/CdS/TiO_2 photocatalysts.

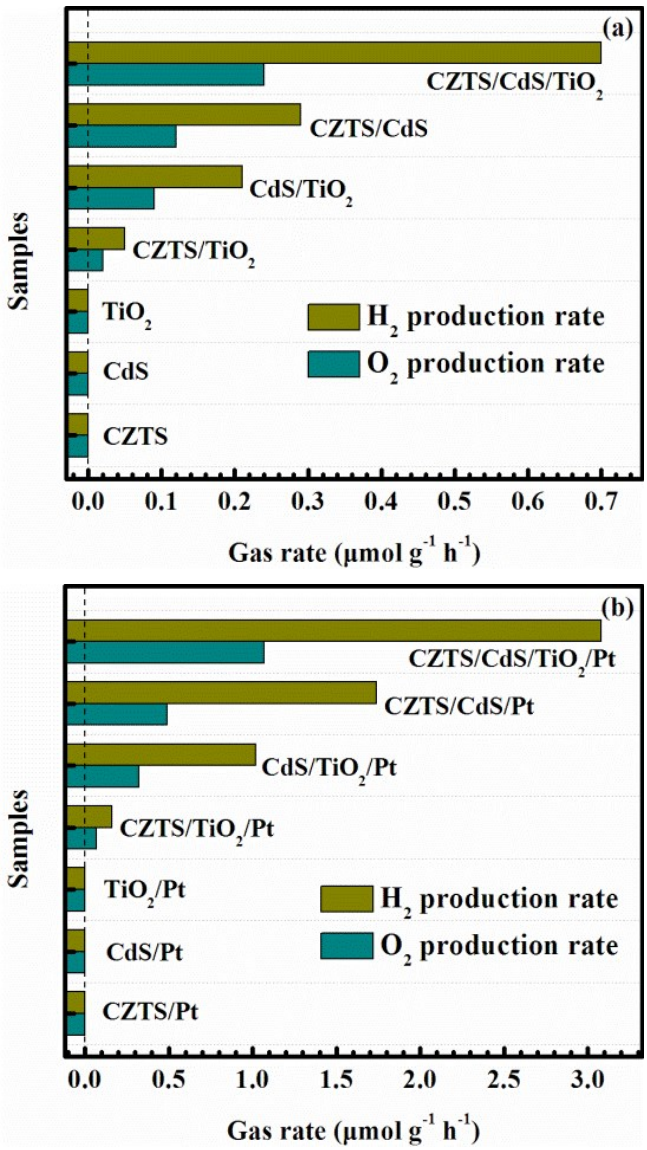

Fig. S15 PWS activity under visible light irradiation: (a) CZTS, CdS, TiO_2, CZTS/TiO_2/Pt, CdS/TiO_2, CZTS/CdS and CZTS/CdS/TiO_2 catalysts; (b) CZTS/Pt, CdS/Pt, TiO_2/Pt, CZTS/TiO_2/Pt, CdS/TiO_2/Pt, CZTS/CdS/Pt and CZTS/CdS/TiO_2/Pt catalysts.

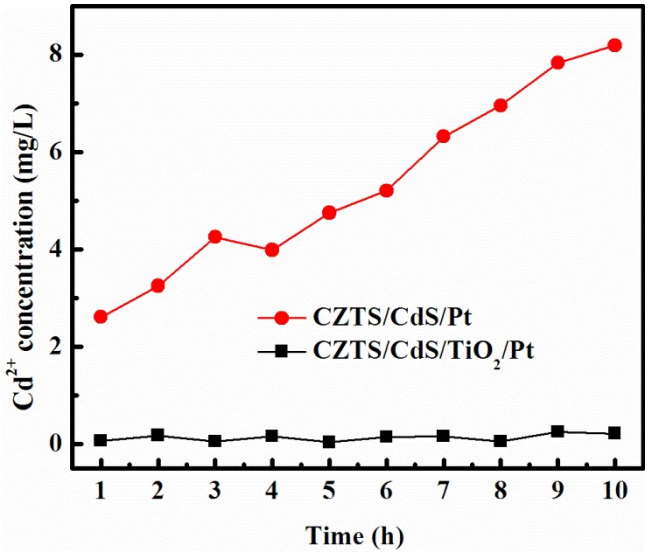

Fig. S16 Cd^{2+} concentration with reaction time in CZTS/CdS/Pt and CZTS/CdS/TiO_2/Pt photocatalytic system.

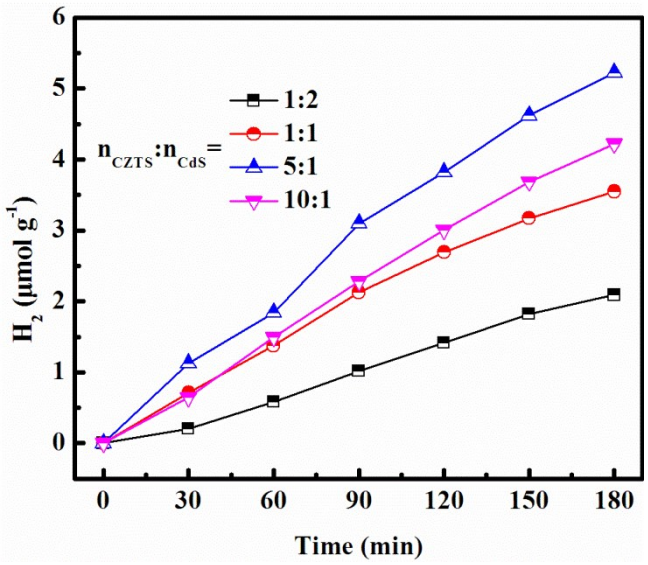

Fig. S17 The effect of CdS buffer layer on PHE activity of CZTS/CdS/Pt under visible light irradiation.

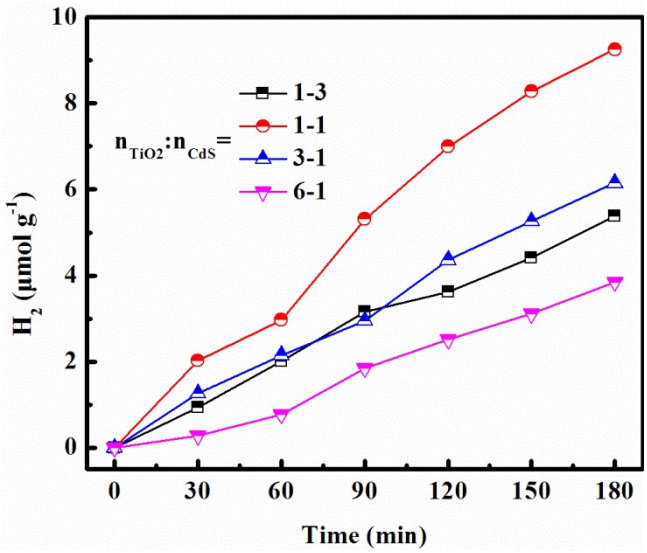

Fig. S18 The effect of TiO_2 protective layer on PHE activity of CZTS/CdS/TiO_2/Pt under visible light irradiation.

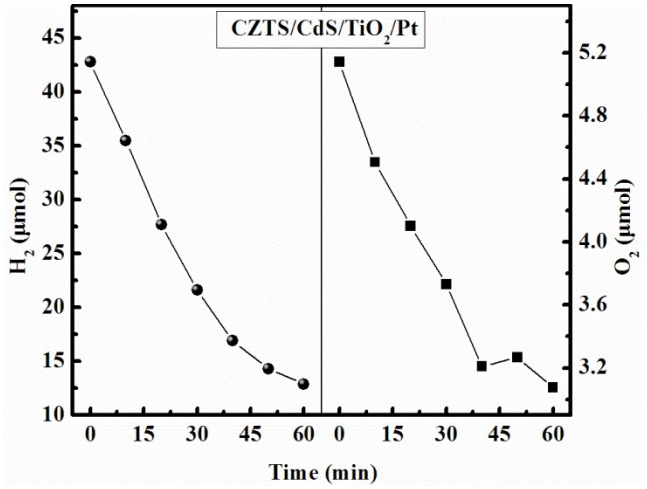

Fig. S19 H_2-O_2 recombination reaction over CZTS/CdS/TiO_2/Pt-water dispersion by injecting 1 mL H_2 and 1 mL O_2 at room temperature in dark condition.

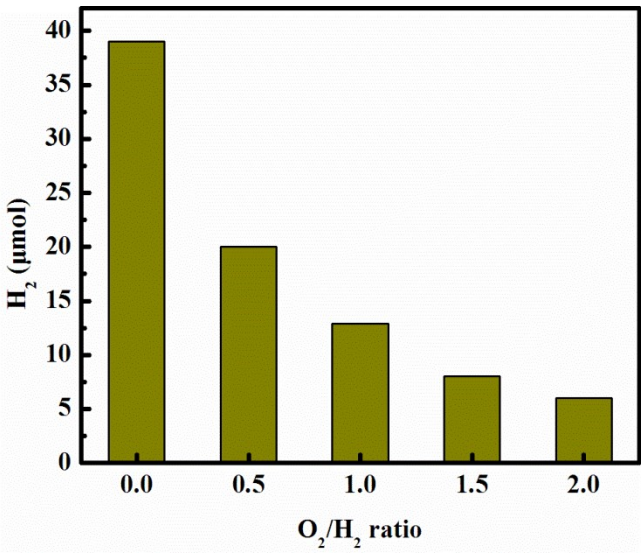

Fig. S20 The recombination experiments of different oxygen partial pressure detected with 1 mL H_2 in a sealed Pyrex flask by injecting different amount of O_2 (0.0, 0.5, 1.0, 1.5 and 2.0 mL) into the 100 mL CZTS/CdS/TiO_2/Pt dispersions.

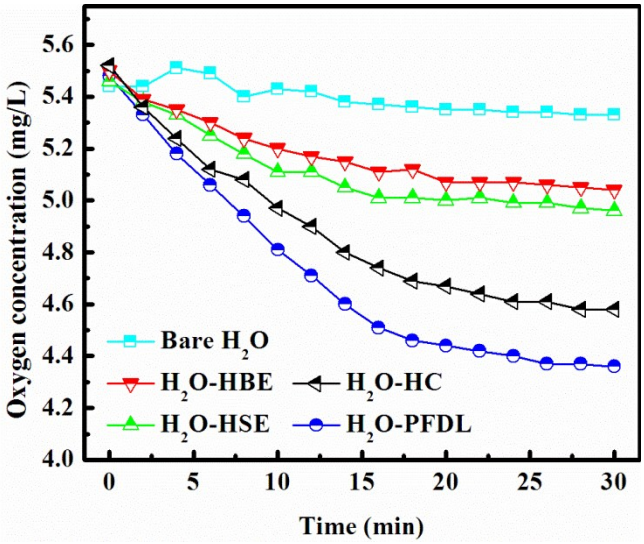

Fig. S21 The oxygen concentration of 100 mL bare H_2O with 350 mg oxygen capture reagents hemin chloride (HC), hemoglobin swinish erythrocytes (HSE), hemoglobin bovine erythrocytes (HBE), and perfluorodecalin (PFDL) at room temperature.

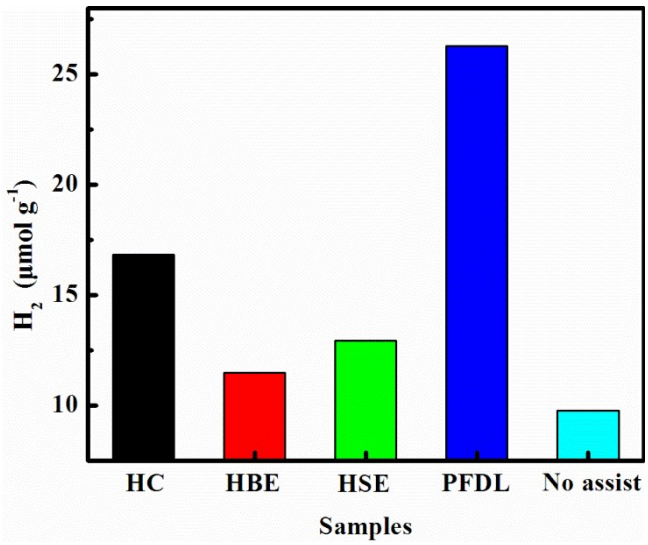

Fig. S22 Photocatalytic hydrogen evolution rate of CZTS/CdS/TiO_2/Pt with different oxygen capture reagents assist, hemin chloride (HC), hemoglobin swinish erythrocytes (HSE), hemoglobin bovine erythrocytes (HBE), and perfluorodecalin (PFDL).

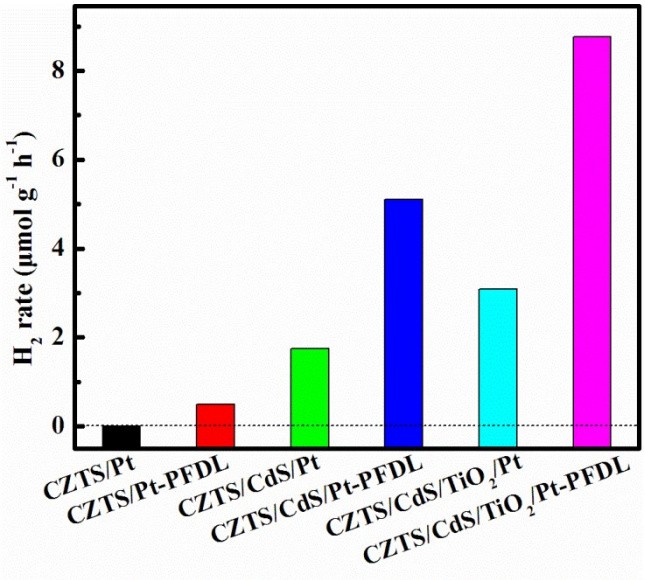

Fig. S23 Comparison of H_2 production rate of CZTS/Pt, CZTS/CdS/Pt and CZTS/CdS/TiO_2/Pt photocatalysts with the PFDL assist under visible light irradiation.